Discrete Element Simulation of Soil Liquefaction: Fabric Evolution, Large Deformation, and Multi-Directional Loading

Gang Wang, Ph.D., P.E., M.ASCE[1]; Duruo Huang, Ph.D.[2]; and Jiangtao Wei, Ph.D.[3]

[1]Dept. of Civil and Environmental Engineering, Hong Kong Univ. of Science and Technology, Clear Water Bay, Kowloon, Hong Kong. E-mail: gwang@ust.hk
[2]Dept. of Civil and Environmental Engineering and Institute for Advanced Study, Hong Kong Univ. of Science and Technology, Clear Water Bay, Kowloon, Hong Kong. E-mail: huangdr@ust.hk
[3]Dept. of Civil and Environmental Engineering, Hong Kong Univ. of Science and Technology, Clear Water Bay, Kowloon, Hong Kong

ABSTRACT

Understanding evolution of microstructure in granular soils can provide significant insights into constitutive modeling of soil liquefaction. By tracing all particle movement, the discrete element modeling (DEM) quantifies the microstructure of a granular assemblage using a variety of fabric indices, such as the numbers of contacts, orientation of contact normal, as well as particles, and voids distribution. The DEM simulations revealed significant change in particle-void fabric to a strongly anisotropic state after initiation of liquefaction. Large flow deformations in the post-liquefaction stage were found to be closely correlated to the evolving particle-void fabric. In addition, fabric evolution in soil packings was also investigated under a variety of multi-directional loading paths. Interestingly, the contact-based fabric ultimately becomes almost identical for all oval and circular loading. The discrete element modeling provides insightful observation that links microscopic fabric evolution to macroscopic cyclic behavior of soils, which is instrumental for developing micromechanically based constitutive models.

INTRODUCTION

Cyclic liquefaction refers to significant loss of strength and stiffness of soils under earthquake shaking. During past earthquakes, large deformation in post-liquefaction process and excessive ground settlements have caused severe damage on civil infrastructure. Granular soils are different from classical continuum media in that they are neither fluid nor solid. In the post-liquefaction stage, granular soils experience large flow deformation in a "fluid-like" state under nearly zero effective stress (Idriss and Boulanger 2008). On the other hand, dilative tendency in the packing may hardens into "solid-like" state to arrest the flow deformation with anisotropy due to contact- and force-networks. Therefore, knowing the particle-scale information of granular particles and void space, collectively termed as "fabric", is crucial for obtaining a fundamental understanding of liquefaction in granular soils. While the geotechnical community has long known that liquefaction results in significant changes in soil fabric, a clear characterization of these changes has been lacking.

Numerical simulations based on Discrete Element Method **(**DEM) provide a more convenient and less costly way to observe the dynamic soil response directly (El Shamy and Zeghal 2007; Andrade et al. 2013). More recently, microstructure and fabric evolution of cyclic liquefaction in granular soils have been studied by tracking particle-void distribution in pre- and post-liquefaction stages (Wang et al. 2016; Wei and Wang 2014, 2016, 2017; Wang and Wei 2016; Wei et al. 2018). The DEM simulations revealed significant change in particle-void distribution

and development of strong anisotropy after initiation of liquefaction.

In this study, large flow deformations in the post-liquefaction stage are found to be closely correlated to the evolving particle-void fabric. Two new void-based fabric measures in terms of shape elongation and orientation anisotropy are proposed to characterize the particle-void fabric during flow liquefaction and cyclic mobility. Evolution of the two new fabric measures are investigated for granular soils over the whole liquefaction process through a series of undrained cyclic simple shear tests using the DEM.

In addition, fabric evolution in soil packing is also investigated under multi-directional loading (circular and oval shearing paths) and the results are compared with the unidirectional loading case. Although zero mean effective stress (initial liquefaction) cannot be achieved for some loading cases, large shear strains are generated within the samples. Interestingly, the samples are evolving towards the same fabric after sufficient loading cycles.

FABRIC EVOLUTION UNDER CYCLIC LOADING

Yade is used to conduct DEM simulation for investigating cyclic behavior of granular soils (Šmilauer et al. 2015). A total of 4000 circular 2D particles are randomly generated within a squared representative volume element (RVE). The radius of particles ranges from 0.15 mm to 0.45mm, while the mean radius R_{50} is 0.3 mm. The simplified Hertz-Mindlin model is used to describe the inter-particle contact behaviors (Yimsiri and Soga 2010). The packing has Young's modulus of 70 GPa and Poisson's ratio of 0.3, which is typical values for quartz sands. Periodic boundary condition is prescribed on the RVE, in order to guarantee the shear strain field to be uniform inside the RVE when a small number of particles are used.

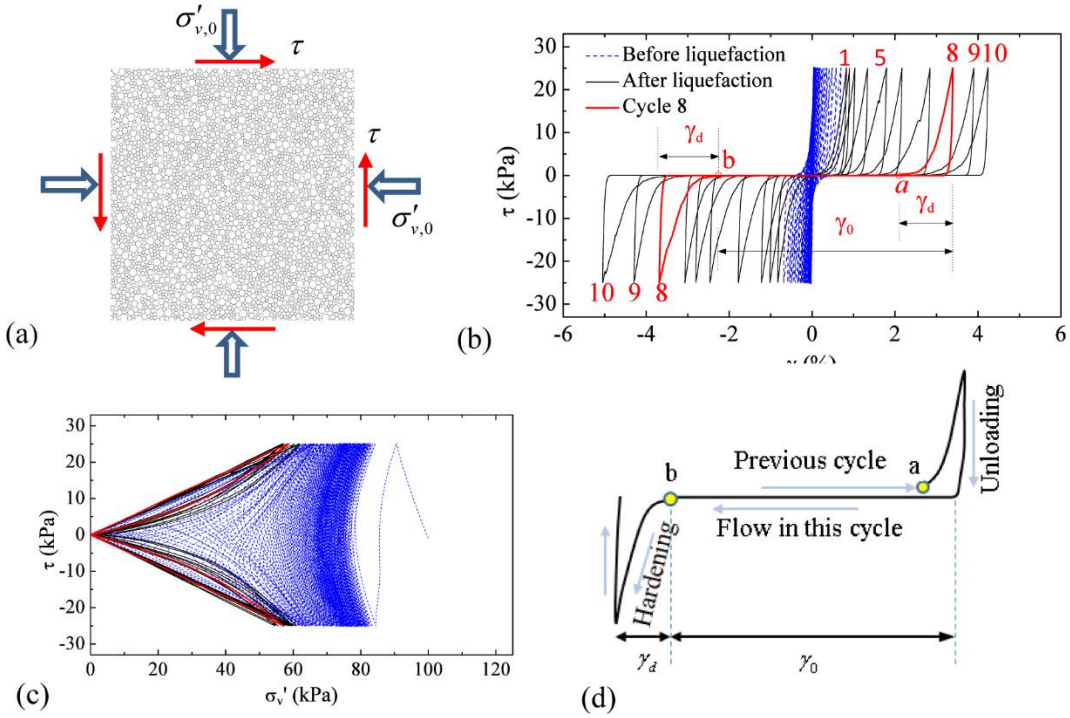

Figure 1. Cyclic stress-strain behaviors of a sample with its relative density of 62%, and cyclic stress ratios (CSR) of 0.25: (a) Model setup, (b) Shear stress and strain curve, (c) stress path, (d) definition of the flow strain and hardening strain. The cycle number is counted from initial liquefaction. (From Wei et al. 2018)

First, the particles are subjected to isotropic consolidation under a confining pressure of 100 kPa, followed by undrained cyclic simple shear tests. Figure 1 shows model setup and simulation results of a sample with its relative density of 62%. It should be noted that "relative density" used in this study is only a nominal terminology to indicate different denseness of the packing in DEM simulation, and it does not have the same meaning as the relative density test performed in the laboratory. It can be observed that with increasing cycle numbers, the effective vertical stress (σ_v') gradually decreases until initial liquefaction occurs. The initial liquefaction is based on the occurrence of zero effective vertical stress, practically, σ_v' <0.5 kPa. After liquefaction, stress path shows repeated "butterfly" loops while the shear strain amplitude keeps increasing cycle by cycle. Figure 1(d) shows the transformation of the packing between a flow state and a hardening state within a loading cycle in the post-liquefaction, where the shear deformation is separated into the flow strain (γ_0) and the hardening strain (γ_d) (Shamoto et al. 1997). To be more specific, the flow strain refers to the double-amplitude strain component when shear stiffness is extremely low and effective stress is almost zero. During flow state, granular packing behaves like "fluid". The hardening strain refers to the strain component when shear stiffness and effective stress have a sharp increase or become much higher than zero. The phase transformation point (point b in Figure 1(d)) represents the end of the flow strain and the start of the hardening strain, when the granular packing becomes dilative and behaves like "solid". At the hardening state, stress strain behavior is almost identical between different loading cycles, while flow strain amplitude increases cycle by cycle. This phenomenon has been well observed in laboratory tests (Idriss and Boulanger 2008; Wang and Wei 2014).

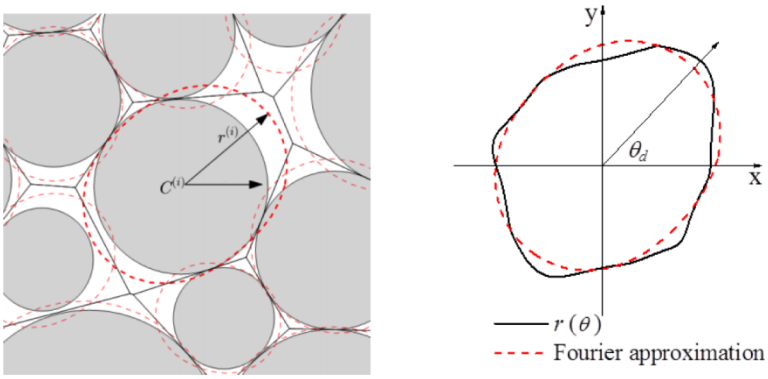

Figure 2. Voronoi tessellation of particle-void cell and Fourier approximation of the void space

Particle-Void Fabric Descriptors

Figure 2 shows Voronoi tessellation of particle-void cell and Fourier approximation of the void space. The cell to particle ratio $r(\theta)$ describes the angular distribution of the ratio between the radial dimension of the cell and the particle. Fourier approximation (Mollon and Zhao 2013) is used to quantify local anisotropy of $r(\theta)$ as the following Equation (1):

$$r^2(\theta) = \frac{A}{\pi}\left[1 + e_d \cos 2(\theta - \theta_d)\right] \quad (1)$$

where A denotes the enclosed area of $r(\theta)$, e_d represents the shape factor controlling the elongation of the void space, and θ_d is the principal orientation of the shape. It is also worth

mentioning that the shape factor (e_d) is important to describe mechanical behaviors of the granular packing. For example, two granular packings with the same void ratio but different e_d values can have different load-bearing structures: Particles that form an arching structure, which is capable of taking loads and behaves like a "solid" have a large value of e_d; Particles that are separated from each other, which cannot take any load and behave like a "fluid" have a very small e_d value.

In this study, a new fabric descriptor E_d is proposed to quantify the partial-void distribution in a granular packing, which is defined as the mean value of e_d,

$$E_d = \frac{1}{N_p}\sum_{i=1}^{N_p} e_d^{(i)} \tag{2}$$

where N_p denotes the number of particles in the packing. Ideally, the probability density function (PDF) of e_d should be used to fully describe the distribution of the shape factor $\{e_d\}$. However, the PDF of the normalized shape factor (e_d / E_d) follows a gamma distribution, which remains to be unchanged for samples under various loading stages. On the other hand, the angular distribution function of θ_d for all particles $f(\theta_d)$ can be expressed using Equation (3):

$$f(\theta_d) = \frac{1}{2\pi}\left[1 + |A_d|\cos 2(\theta_d - \Theta_d)\right] \tag{3}$$

where $|A_d|$ quantifies the anisotropy degree of $f(\theta_d)$; $\Theta_d \in (0, \pi)$ is the principal direction of $f(\theta_d)$. The sign of A_d is determined by Θ_d such that when $\Theta_d \in (0, \pi/2)$, $A_d > 0$ and when $\Theta_d \in (\pi/2, \pi)$, $A_d < 0$.

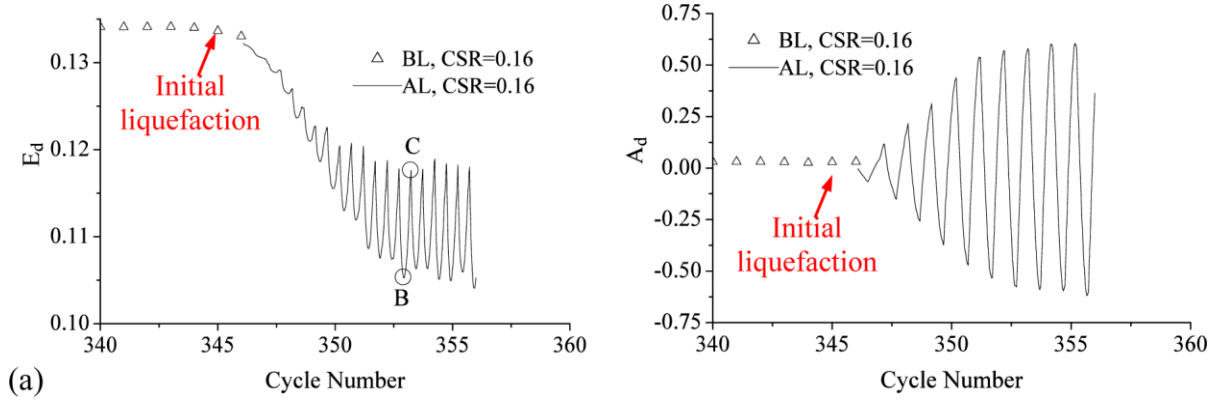

Figure 3. The evolution of E_d and A_d over numbers of cyclic loading during post-liquefaction

Particle-Void Evolution in Pre- and Post-Liquefaction Stages

Descriptors E_d and A_d are derived to quantify the particle-void fabric based on statistical analyses of shape factor and principal direction associated with all particles in the packing. The evolution of the descriptors before and after initial liquefaction is examined in the current study. Figure 3 shows the evolution of E_d and A_d over the number of loading cycles under different cyclic stress ratios (CSR). It can be observed that before initial liquefaction, the change in the

fabric descriptors is negligible, while it becomes significant after the initial liquefaction. During the eight loading cycles after initial liquefaction, E_d decreases from 0.133 to 0.105 while the amplitude of A_d increase from 0.03 to 0.6. Afterwards, evolution of both E_d and A_d get stabilized. Within each loading cycle, E_d changes from 0.105 to 0.117 and A_d varies from -0.6 to 0.6, indicating the existence of an ultimate state of particle-void distribution. The decrease in E_d indicates that local void distribution around single particle (e_d) on average becomes less anisotropic.

In the post-liquefaction stage, granular packing transforms from the flow state to hardening state under shearing, a phenomenon termed as "jamming transition" in the physics community. Here, the jamming transition specially refers to phase transformation at a fully liquefied state. The transition point is defined to separate the flow strain and the hardening strain as illustrated in Figure 1(d). To identify the transition points, the coordination number Z is defined as the ratio between total inter-particle contact number and total particle number in the assemblage (Wang and Wei 2016). Figure 4(a) shows evolution of two fabric descriptors E_d and A_d during cyclic loading for sample Dr=62%. Given that the change in E_d and A_d is negligible before initial liquefaction, we only plot data in the post-liquefaction stage. It can be observed that E_d decreases gradually with increasing of absolute A_d. The jamming transition point (Z = 2) and intermediate point (Z = 1) are highlighted using red circles. The jamming transition point distinctly defines loci of a hardening state line (HSL) in the E_d-A_d space. Note that the conventional phase transformation line is defined in the p'-q space for the transition between the dilative and contractive response of the soil (Wang and Xie 2014). The HSL line specifies the phase transformation from the flow state to hardening state at the fully liquefied stress state (mean effective stress approaches 0) in terms of fabric descriptors.

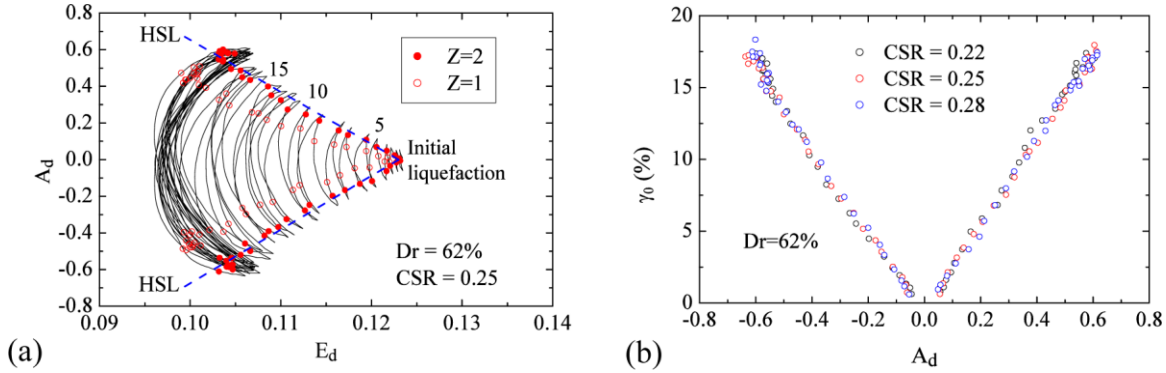

Figure 4. (a) Evolution of E_d and A_d in the post-liquefaction stage, (b) relationship between A_d and γ_0 under different loading conditions

Inside the hardening state line, the granular packing belongs to the flow state which doesn't take load and behaves like a fluid. Beyond the hardening state line, the granular packing is believed in a hardening state with a stable load-bearing structure and behaves like a solid. The existence of HSL also indicates the fact that the loading bearing structure in the post-liquefaction stage can be only formed if either E_d or $|A_d|$ is sufficiently large. Otherwise, the packing remains in a flow state. In addition, the relationship between flow strain amplitude and the fabric descriptor A_d has been developed. Figure 4 (b) shows the A_d - γ_0 relation for a Dr=62% sample under different loading paths. Interestingly, data from different loading paths (i.e. CSR=0.22, 0.25 and 0.28) align on two symmetric lines, indicating that the A_d - γ_0 relation is independent of

different loading conditions

FABRIC EVOLUTION UNDER MULTI-DIRECTIONAL LOADING

During earthquake shaking, the shear wave propagated through the ground is essentially irregular. Consequently, cyclic loading applied on the soil element is multi-directional, which involves variation in both loading direction and loading amplitude (Ishihara, 1996). As shown in the previous sessions, uni-directional cyclic simple shear tests are usually performed in laboratory or by numerical simulations. Yet, the influence of multi-directional loading is often unclear.

The evolution of fabric under multi-directional loading is also investigated in the current study. Figure 5(a) shows a three-dimensional DEM medium-dense packing, with a total number of 10000 spherical particles randomly generated in the RVE. Periodic boundary is prescribed on this RVE to eliminate the non-uniformity caused by RVE boundary. Particle radius ranges from 0.225mm to 0.45mm. Hertz-Mindlin contact model is employed to describe the force-displacement behavior between contacted particles. In the contact model, Young's modulus E and Poisson's ratio are set as 70GPa and 0.3 respectively. The packing is initially subjected to an isotopically consolidation under the confining pressure (p_0) of 100 kPa, followed by undrained multi-directional cyclic simple shear test as shown in Figure 5(b). The applied shear stress components (τ_x and τ_y) vary according to the trajectories illustrated in Figure 5(c). To measure the extent of multi-directionality of the loading, an aspect ratio, *AR*, is defined as $AR = \max\|\tau_y\| / \max\|\tau_x\|$. Clearly, the case of *AR*=0 represents the uni-directional loading. When *AR* equals to 1, the loading path is circular. An oval loading path is indicated by $0 < AR < 1$. In all the simulations, we assume the amplitude of τ_x is 25 kPa, the amplitude of τ_x varies from 0 to 25 kPa.

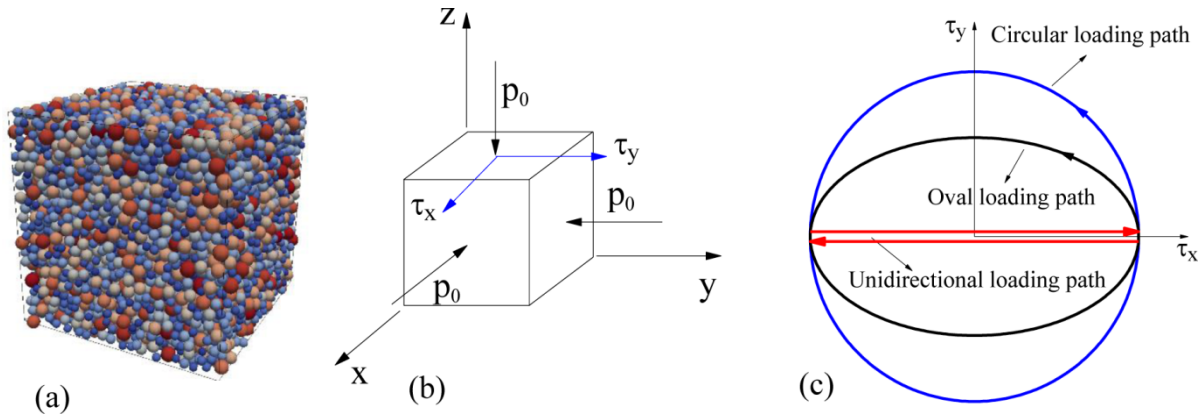

Figure 5. (a) Three-dimensional DEM packing; (b) applied stress; (c) loading paths

Figure 6 shows the effective stress path ($\tau = \sqrt{\tau_x^2 + \tau_y^2}$) under circular loading (*AR*=1), oval loading (*AR*=0.6) and unidirectional loading (*AR*=0). As the cycle number increases, the effective vertical stress gradually decreases due to the increase of excess pore water pressure. Note that the effective stress barely approaches the critical state line (CSL) without going down to zero for the circular and oval loading cases, indicating that the samples are not fully liquefied. Figure 7 demonstrates development of shear strain under circular, oval and unidirectional

loading. Development of large shear stain can be observed and reach 20%. It is also worth mentioning that the maximum shear strain developed in uni-axial loading is approximately in the order of 20%. Coordination number and contact based fabric tensor can be employed to quantify the internal load bearing structure of granular packing. In particular, the contact based fabric tensor adopted here (Guo and Zhao 2013) is a second order tensor that constructed by the following Equation (4):

$$\phi_{ij} = \frac{1}{N_c}\sum_{k=1}^{N_c} n_i^{(k)} n_j^{(k)} = \begin{bmatrix} 1/3 & 0 & \phi_{xz} \\ 0 & 1/3 & \phi_{yz} \\ \phi_{zx} & \phi_{zy} & 1/3 \end{bmatrix} \tag{4}$$

where **n** is the contact normal vector. It can been verified from simulation results that the diagonal components ϕ_{xx}, ϕ_{yy} and ϕ_{zz} are close to 1/3 and off-diagonal components ϕ_{xy} is close to zero.

Therefore, ϕ_{zx} and ϕ_{zy} are the only two components that need to be assessed.

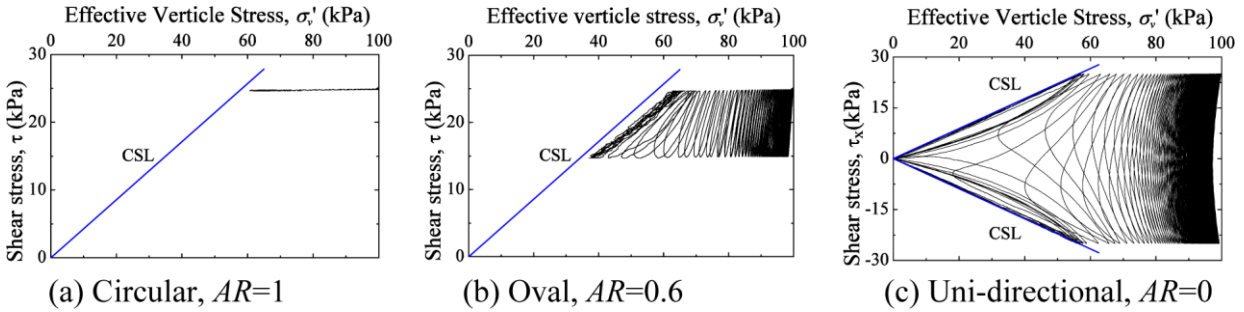

(a) Circular, *AR*=1 (b) Oval, *AR*=0.6 (c) Uni-directional, *AR*=0

Figure 6. Effective Stress paths under (a) circular loading (AR=1), (b) oval loading (AR=0.6) and (c) unidirectional loading (AR=0)

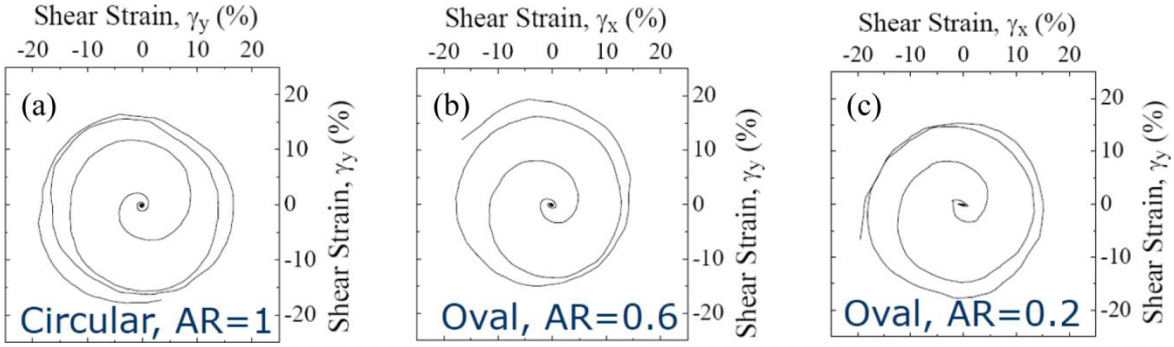

Figure 7. Development of shear strain under (a) circular loading (AR=1), (b) oval loading (AR=0.6) and (c) oval loading (AR=0.2)

Figure 8 presents the contact-based fabric component ϕ_{zx} versus ϕ_{zy} in the circular and oval loading tests. For the circular loading path, fabric trajectory starts from a small circle and gradually expands as the cycle number increases. For these oval loading paths, fabric trajectory starts from an oval and gradually expands to a bigger circle with the increase of cycle number. The fabric trajectory is centred in the origin. It is interesting to find that a same "stable state" of the contact-based fabric will be reached regardless of loading path in oval/circular loading. Although not reported in this paper due to limited space, a "stable state" of coordination number

and particle-void fabric was also found to be reached in oval/circular loading after sufficient number of loading. In general, the cycle number inducing large strains (i.e. 3% of shear strain amplitude) decreases with the increase of AR for oval loading conditions based on numerical simulation.

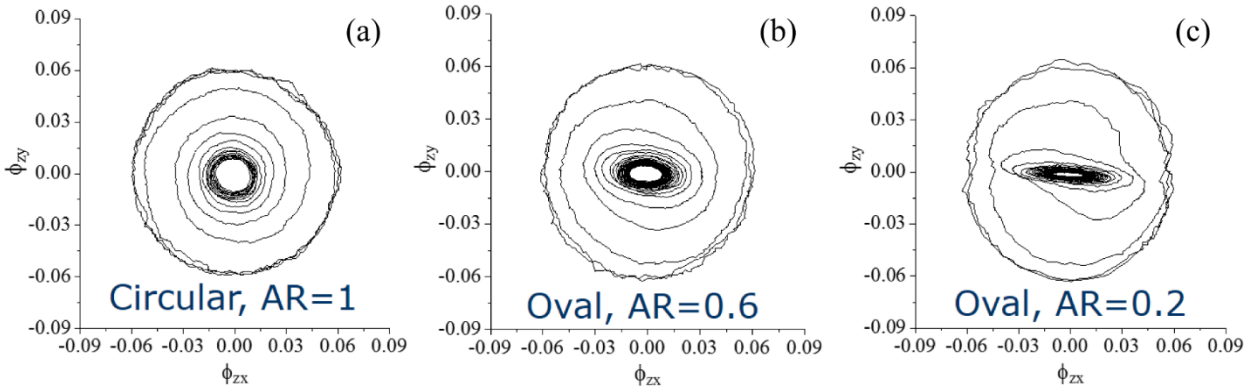

Figure 8. Development of contact-based fabric component under (a) circular loading (AR=1), (b) oval loading (AR=0.6) and (c) oval loading (AR=0.2)

CONCLUSION

In this study, the particle-void distribution of granular packing is quantified using two newly developed microscale descriptors, E_d and A_d, which measure the shape and orientation of local void distribution during cyclic liquefaction. It was observed that the change in the void-based fabric is *irreversible* and is primarily developed in the post-liquefaction stage, accompanied by increasing post-liquefaction deformation. After initial liquefaction, evolution of E_d and A_d has been identified as E_d decreases and $|A_d|$ gradually increases cycle by cycle. In the post-liquefaction stage, jamming transition could occur in the granular flow, which transforms the granular assemblage from a "fluid-like" state to a "solid-like" state to arrest the flow deformation. Our study is the first to discover a *hardening state* line (HSL), defined in the void-fabric space, that delineates the boundary between a flow state and a jamming/hardening state when the soil is fully liquefied. The concept is somewhat related to conventional phase transformation defined in the stress space, but our emphasis is on the case that the mean effective stress approaches zero. The post-liquefaction deformation of the granular packing is strongly correlated to the evolution of fabrics, so fabric indices can be used to quantify the amplitude of flow deformation. Finally, a *stable state* of particle-void distribution can be achieved in post-liquefaction after sufficient number of loading cycles, which is influenced by packing density but not by loading paths.

The multi-directional loading behaviors of granular soils were explored using three-dimensional DEM simulations. Under circular/oval shear loading, the packing will not experience liquefaction even though large shear deformation can be developed. Evolution of contact-based fabric trajectory starts from a shape similar to the shear stress path to a "stable state" circle, which is almost identical for all oval and circular loading tests. A stable state of coordination number and particle-void fabric is also observed.

It is worth clarifying that "stable state" in the above observation specifically refers to the phenomenon that the evolution "pattern" of stress-strain and fabric would not change during repeated cyclic loading. The notion should not be confused with the critical state or steady state

concept of sands in the literature (Been et al. 1991). The discrete element modeling provides insightful observation that links microscopic fabric evolution to macroscopic behavior of soils in the liquefaction process, which is instrumental for developing micromechanically based constitutive models.

ACKNOWLEDGEMENTS

This study was financially supported by Theme-based Research Scheme Grant No. T22-603-15N, General Research Fund No. 16213615 from the Hong Kong Research Grants Council, and Initiation Grant No. IGN17EG01 from the University Grants Committee (UGC). The support is gratefully acknowledged.

REFERENCES

Andrade, J.E., Mital, U. and Mohammadnejad, T. (2013). "Micromechanical Origin of Static and Dynamic Liquefaction in Granular Soils." *Proceedings of the Fifth Biot Conference on Poromechanics*, Vienna, Austra, 2013

Been, K., Jefferies, M.G., Hachey, J. The critical state of sands. *Géotechnique* 41 (3), 365-381.

El Shamy, U., and Zeghal, M. (2007). "A micro-mechanical investigation of the dynamic response and liquefaction of saturated granular soils." *Soil Dynamics and Earthquake Engineering* 27, 712–729.

Idriss, I., and Boulanger, R.W. (2008). *Soil liquefaction during earthquakes*, EERI monograph series, No. MNO-12. Oakland, CA, USA.

Ishihara, K. (1996). *Soil behaviour in earthquake geotechnics*. Oxford: Clarendon Press.

Guo, N. and Zhao, J. (2013). "The signature of shear-induced anisotropy in granular media." *Comput. Geotech.* 47, 1-15.

Mollon, G., and Zhao, J. (2013). "Generating realistic 3D sand particles using Fourier descriptors." *Granular Matter*, 15(1), 95-108.

Shamoto, Y., Zhang, J., and Goto, S. (1997). "Mechanism of large post-liquefaction deformation in saturated sand." *Soils and Foundation*, 37(20), 71-80.

Šmilauer, V et al. (2015). Using and Programming. In Yade Documentation 2nd ed. The Yade Project, DOI 10.5281/zenodo.34043 (http://yade-dem.org/doc/)

Wang, G. and Wei, J. (2016). "Microstructure evolution of granular soils in cyclic mobility and post-liquefaction process." *Granular Matter*, 18(3), 51.

Wang, G. and Xie, Y. (2014). "Modified bounding surface hypoplasticity model for sands under cyclic loading." *Journal of Engineering Mechanics* ASCE, 140 (1), 91-101.

Wang R., Fu P., Zhang J.M., Dafalias Y.F. (2016). "DEM study of fabric features governing undrained post-liquefaction shear deformation of sand." *Acta Geotechnica* 11(6), 1321–1337.

Wei, J. and Wang, G. (2014). "Cyclic Mobility and Post-liquefaction Behaviors of Granular Soils under Cyclic Loading: Micromechanical Perspectives." *Proc. 10th US National Conference on Earthquake Engineering*, Anchorage, Alaska, July 21-25, 2014.

Wei, J., and Wang, G. (2016). "Evolution of fabric anisotropy in cyclic liquefaction of sands." *Journal of Micromechanics and Molecular Physics* 1, 3 & 4, 1640005, 2016.

Wei, J., and Wang, G. (2017) "Discrete-element method analysis of initial fabric effects on pre- and post-liquefaction behavior of sands." *Géotechnique Letters*, 7(2), 1-6.

Wei, J., Huang D., Wang G. (2018). "Micro-scale descriptors for particle-void distribution and jamming transition in pre- and post-liquefaction of granular soils." *Journal of Engineering Mechanics* ASCE, accepted.